POLITECNICO DI TORINO
Repository ISTITUZIONALE

Large-scale cryostructures and pedogenesis in blockstreams in the Ligurian Alps (NW Italy): Pleistocene paleoclimate implications

Original
Large-scale cryostructures and pedogenesis in blockstreams in the Ligurian Alps (NW Italy): Pleistocene paleoclimate implications / D'Amico, Michele Eugenio; Pintaldi, Emanuele; Colombero, Chiara; Bonifacio, Eleonora; Benech, Andrea; Freppaz, Michele. - In: CATENA. - ISSN 0341-8162. - 249:(2025). [10.1016/j.catena.2024.108676]

Availability:
This version is available at: 11583/2999041 since: 2025-04-10T14:25:52Z

Publisher:
Elsevier B.V.

Published
DOI:10.1016/j.catena.2024.108676

Terms of use:

This article is made available under terms and conditions as specified in the corresponding bibliographic description in the repository

Publisher copyright

(Article begins on next page)

15 May 2025

Catena 249 (2025) 108676

Contents lists available at ScienceDirect

Catena

journal homepage: www.elsevier.com/locate/catena

Large-scale cryostructures and pedogenesis in blockstreams in the Ligurian Alps (NW Italy): Pleistocene paleoclimate implications

Michele Eugenio D'Amico [a], Emanuele Pintaldi [b,*], Chiara Colombero [c], Eleonora Bonifacio [b], Andrea Benech [b], Michele Freppaz [b]

[a] Università degli Studi di Milano – DISAA, Via Celoria 2, Milano, Italy
[b] Università degli Studi di Torino – DISAFA, Largo Braccini 2, Grugliasco, TO, Italy
[c] Politecnico di Torino – DIATI, Corso Duca degli Abruzzi 24, Torino, Italy

ARTICLE INFO

Keywords:
Clay minerals
Cryoturbation
Podzol
Soil micromorphology

ABSTRACT

Blockstreams and blockfields are periglacial features induced by strong frost-action processes. As their formation can be associated with specific environmental conditions such as permafrost (in absence of an impermeable layer below), these landforms have been recognized worldwide as key factors in paleoclimate reconstructions. However, their internal morphology and origin, especially in alpine environments, were poorly investigated. In particular, the fine material at their base has almost never been characterized from the pedogenic point of view.

We opened and described a 12 m-wide, 3 m-deep soil transect inside and between two blockstreams in the Ligurian Alps (NW Italy); we took samples from each pedogenic horizons and analysed them to obtain chemical, physical, mineralogical, and micromorphological data.

The soil transect was characterized by deep involutions likely caused by ancient, deep cryoturbation associated to former ice-rich permafrost and its collapse during thawing (load casting). Many other macro- (i.e. large platy structure, fragic properties, vesicular porosity, wedge cast-like structures, Fe-Mn nodules above a permeable layer) and micro-morphological features (i.e. Fe-Mn concentrations, fractured clay coatings, silt caps) evidence ice-rich permafrost, while the intensity of pedogenesis points to a particularly long soil forming processes and preservation of soil materials during different Pleistocene glacial and interglacial periods.

1. Introduction

Blockstreams and blockfields are periglacial features induced by strong frost-action processes, such as frost-shattering, frost sorting, frost heave (e.g., Karte, 1983, Goodfellow, 2007; Ballantyne, 2010). As their formation can be associated with specific environmental conditions such as permafrost (e.g., Karte, 1983, D'Amico et al., 2019), these Pleistocene fossil periglacial features are considered key indicators of relict non-glacial surfaces (Goodfellow, 2007) and have been used in paleoclimatic reconstructions (e.g., Ballantyne, 1998; André et al., 2008; Wilson, 2013; Pintaldi et al., 2021a). Indeed, although polygenetic (i.e. derived from several frost-action or temperate/warm temperature weathering processes) (André et al., 2008; Wilson, 2013), the genesis of blockstreams and blockfields is commonly related to the occurrence of permafrost (Harris, 1994). Blockstream formation could be also associated with deep seasonal freezing if an impermeable layer limits water percolation and increases the pressure exerted by freezing water in the overlying loose materials (Van Vliet-Lanoë, 1998). Although sometimes active, especially at high elevation (e.g., Pintaldi et al., 2021b), most of these periglacial landforms have been described in the literature as relict features (Wilson, 2013), because present-day climatic conditions are usually not suitable for their formation or activity. Indeed, as reported by several authors worldwide (e.g., Barrows et al., 2004, Hansom et al., 2008, Wilson et al., 2008) such periglacial features are generally very old, ranging from ~ 20 to over 700 ka and occur mainly in areas adjacent to but beyond the margins of the (global) Last Glacial Maximum (LGM; ~23 ka) glaciers (Wilson, 2013). At that time these areas were characterized by extremely cold periglacial climate conditions and blockstreams/blockfield formation represented therefore one response of the landscape to those conditions (e.g., Clark and Ciolkosz, 1988; Boelhouwers, 1999).

Despite their paleoclimatic significance, the internal pedogenic organization of blockfields and blockstreams has been seldom described. In particular, to our knowledge, only 33 from 113 available studies, from

* Corresponding author.
E-mail address: emanuele.pintaldi@unito.it (E. Pintaldi).

https://doi.org/10.1016/j.catena.2024.108676
Received 5 April 2024; Received in revised form 2 December 2024; Accepted 13 December 2024
Available online 15 December 2024
0341-8162/© 2024 The Authors. Published by Elsevier B.V. This is an open access article under the CC BY license (http://creativecommons.org/licenses/by/4.0/).

ca.1950 to 2023, show some information on the fine materials at the base of the blockstreams and blockfields, the others dealing only with their location and surface analysis (Table S1). From these 33 studies, most show granulometric composition, fewer characterize mineralogy, weathering degree and cryogenic structures. Soil horizons have been characterized in only less than 10 studies (table S1). Mineralogy and weathering degree have been used to estimate the relative age of blockfields in many areas, but not pedogenesis. From a morphological point of view, such periglacial landforms show an upper layer made up of coarse stones, often imbricated, whose size becomes smaller with depth; organic matter-rich "soil" material appears at 0.2–0.6 m depth, followed by brownish or reddish-brown silty sand or loamy layers (Andersen et al., 2018; Grab, 1999; Wilson 2007, 2013; Paro 2011; Pintaldi et al., 2021a). However, detailed pedogenic descriptions of the soil materials are available in the literature in only a handful of cases. For example, André et al. (2008) showed how the fine materials below and between the Falkland stone runs were composed of a mixture of extremely well-developed Fe-rich materials derived from previously weathered soils, enriched in organic matter in the upper parts. Hopkinson and Ballantyne (2014) showed the internal structure, the granulometry, the chemical composition and clay mineralogy of the fine fraction in the matrix-supported base of blockstreams in Scotland, but no pedogenic characterization was given. Caine's study in Tasmania (Caine 1966) described strongly weathered, clay-rich materials at the bottom of the blockstreams, overlain by less weathered brown materials rich in pedorelicts, followed by a black organic matter-rich horizon just below the surface stone layers. More recently, Marr and Löffler (2017) described soil horizons under blockstreams and blockfields in Norway, showing the weathering degree of the brownish or greyish fine materials and their differentiation in different horizons. The characterization of the orientation and weathering degree of the stone fragments in the basal part of the blockstreams is seldom given as well (e.g., Pintaldi et al., 2021b).

A detailed characterization of the distribution and genesis of the pedogenic horizons inside and between blockstreams is thus missing worldwide. Preserved pedogenic horizons, materials, clay minerals and Fe oxides are important tools for reconstructing geomorphic dynamics in mountain areas (e.g. Masseroli et al., 2020). Moreover, the orientation of stones at depth below the blockstreams, the structural aggregation and the spatial distribution of stone-rich layers and pedogenic horizons might give important hints about the cryogenic movements associated with blockstreams development. They might also indicate soil forming environments during the time scale in which the blockstreams developed, both during cold periods and previous warm ones (e.g. André et al. 2008), possibly confirming the hypothesis that many blockstreams and blockfields are polygenetic geomorphic features often formed thanks to a previous weathering of the substrate in temperate or in tropical-subtropical environments.

By characterizing the internal structure and pedogenesis of a slope section inside blockstreams and in the space between them in the Ligurian Alps (SW Italian Alps), our aim is to understand the environmental conditions during the formation of this landform. This will help reconstructing paleoclimatic conditions in Alpine areas, which are often difficult to characterise. Given the good preservation of the observed soil section, the results will be also useful to understand possible formation processes of blockstreams and their distribution in mountain slopes.

2. Materials and methods

2.1. Study area

Bric Mindino peak (1879 m a.s.l.) is located in the Ligurian Alps (Fig. 1), separating Tanaro, Casotto and Mongia valleys. Most of the Ligurian Alps were unglaciated during the Pleistocene, excluding the highest areas, often bearing cirques, and some of the northbound valleys. The Equilibrium Line Altitude (ELA) in the Western Alps during LGM was around 1850–2000 m a.s.l. (Carraro and Giardino, 2004; Federici et al., 2012). Although close to the lower limit of the ELA, no cirques, glacial erratics, moraines, roches moutonnèes or other glacial geomorphological features can be found on Bric Mindino, indicating that it was not glaciated. In addition, Bric Mindino is characterized by rounded morphologies and cryoplanation terraces (D'Amico et al.,

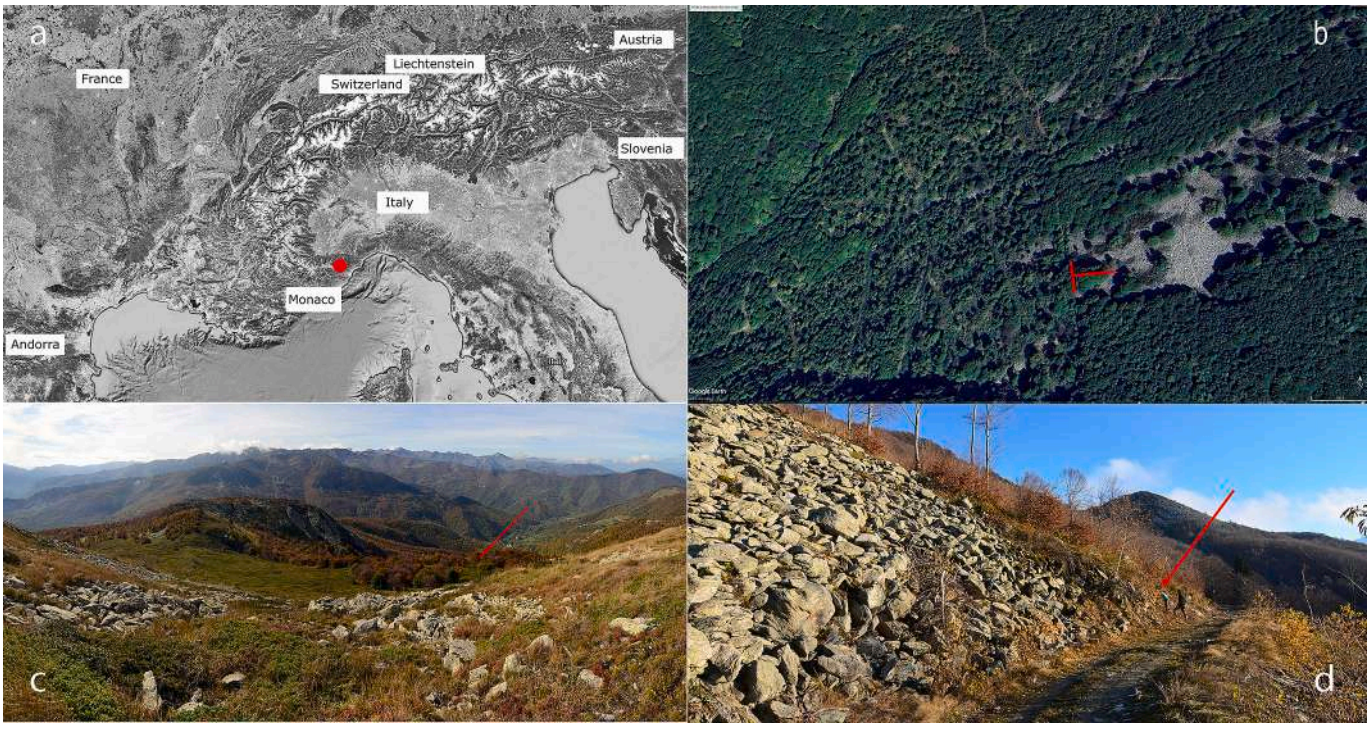

Fig. 1. Location of Bric Mindino (a), on whose north-western slopes (b, c) we observed a soil transect (indicated by the arrow) between the blockslope deposit (d) on the immediate north and a blockstream (further down the road). The location of the two Eletric Resistivity Tomography sections is indicated by the red lines in (b).

2019). Extensive blockfields occur in the flattest areas, partly covered by vegetation, and blockstreams and blockslopes (sensu van Steijn et al., 2002) on the steepest slopes. In particular, the north-western slope is covered by large-scale sorted stripes/blockstreams/blockslopes, composed of a repeated pattern of 4–15 m wide sectors composed of lichen-covered, imbricated stones and boulders, separated by 8–25 m of well vegetated areas. The vegetated area is, however, covered by a thin block cover as well, which is partly not visible because of quite thick litter and mosses layers (Fig. 2a). No rock outcrops are visible in the source areas upslope. The length of the blockstreams is between 35 and 370 m. Small ridges, furrows and lobate forms characterise the surface of the blockstreams along the slope gradient, suggesting flow (e.g. Slee et al., 2023).

Extensive cryoturbation and evidences of permafrost at different depths have been observed in soils on the Bric Mindino slopes (D'Amico et al., 2016; 2019); on the flattest surfaces, strongly polygenetic soils indicate very different paleoclimatic conditions, from warm and humid subtropical to permafrost conditions (D'Amico et al., 2016).

The lithological substrate is metamorphic rhyolitic porfiroids, slightly laminated, characterized by high hardness and high quartz content, associated to micas and K-feldspars (Vanossi, 1990).

We exploited one of the forest road dissections to observe a 12 m-wide, 3 m-deep soil transect between a relict blockstream, in a valley bottom, and a blockslope, at an elevation of 1460 m a.s.l.. The slope steepness is around 25°, its orientation is west. Present-day mean annual air temperature at this elevation in the Ligurian Alps is around 5.4 °C (data based on nearby Ormea weather station located at 730 m a.s.l. considering the standard lapse rate of 6 °C km^{-1}, Biancotti et al., 1998). The mean air temperature in the coldest month is around −4 °C. Average yearly rainfall is around 1090 mm (in nearby Ormea, Biancotti et al., 1998), with maxima in spring and fall and a summer minimum indicating Mediterranean influences; however, frequent afternoon fogs increase soil humidity on the highest slopes during the driest months.

Present day vegetation on Bric Mindino, and on the soil section, is open beech (*Fagus sylvatica* L.) forest with *Vaccinium myrtillus* L. and *Rhododendron ferrugineum* L. in the understory. At higher elevations, heath with *Calluna vulgaris* and other ericaceous dwarf shrubs is widespread. The forests are managed as coppice, and many forest roads have been recently opened disturbing the natural topography. As in large areas of the Ligurian Alps on quartzitic substrates (IPLA, 2007), most soils are Podzols, despite the broadleaf vegetation, evidencing a particularly base-poor parent material. In forests, Albic Podzols are the most common soil type, while under grassland and heath Umbric Albic Podzols are more common. On flat surfaces, intense stagnic properties associated to cemented placic horizons are common (D'Amico et al., 2016).

2.2. Field activities and physical, chemical, and mineralogical analysis

We cleaned the face of the roadcut by removing ca. 1 m of loose materials deposited by erosive processes, to observe all pedogenic horizons and morphologic structures inside the blockstream. The field description of the soil horizons was performed according to FAO (2006), and the soil classified according to IUSS Working Group WRB (2022). In a few cases, we added some qualifiers to specific soil horizons in brackets, to indicate minor but peculiar and clearly detectable characteristics. We then sampled all genetic horizons to perform some chemical and physical analyses, according to standard methods (Van Reeuwijk, 2002). Soil pH was measured in a 1:2.5 soil–water extract. The particle-size distribution was obtained by the pipette method after organic matter destruction with H_2O_2 followed by dispersion with Na-hexametaphosphate. Total carbon (corresponding to total organic carbon-TOC due to the absence of carbonates) and nitrogen (TN) concentrations were measured by dry combustion (3 replicates) with an elemental analyzer (CE Instruments NA2100, Rodano, Italy). Oxalate-extractable Fe and Al (Feo and Alo), and dithionite-extractable Fe (Fed) were measured with Flame Atomic Absorption Spectroscopy (Analyst 400, Perkin Elmer, Waltham, MS, USA), on selected horizons to obtain indicators of the intensity of pedogenic development.

The mineralogical investigations were carried out using a Philips PW1710 X-ray diffractometer (40 kV and 10 mA, CoKα radiation, graphite monochromator) on selected horizons. The divergence and receiving slits were set at 1 and 0.2 °2θ, respectively. The clay fraction (< 2 μm) was separated by sedimentation, flocculated with $MgCl_2$, washed until free of Cl-, and freeze-dried. Scans were made from 3 to 35 °2θ at a speed of 1 °2θ min^{-1}, on air dried (AD), ethylene glycol solvated (EG), and heated oriented mounts, following the methods of the Italian Soil Science Society (Mirabella et al., 2005). The presence of chlorite was ascertained by the presence of a peak at 1.4 nm upon heating to 550 °C, illite was recognized by its peak at 1.0 nm on the AD sample, while the appearance of a peak at 1.6 nm (or at lower angles) in the EG-saturated specimen was taken as an evidence of the presence of smectite. The presence of vermiculite, kaolinite and hydroxy-interlayered minerals (HIV and/or HIS) was ascertained by comparing the XRD patterns obtained after heating the samples to 350 and 550 °C, in addition to AD, Mg and EG. A semi-quantitative evaluation of mineral abundance was performed using the Mineral Intensity Factors method reported by Islam and Lotse (1986) which considers peak intensities and is suitable for oriented samples.

The presence of short-range-order allophane or imogolite-type materials (ITMs) was assessed by measuring the pH in 1 M NaF (1:50) solution; values above 8.5 were considered a positive indicator of their presence (Burt, 2004).

The micromorphology of one horizon of unclear genesis (Bsm(v)) was examined in thin sections produced from strongly cemented aggregates under the optical microscope Carl Zeiss Axioscope A1 equipped with Axiocam MR5 camera and AxioVision 4.8.2 software (Germany), at the Puschino Lab (Moscow, Russia). The description was performed based on Verrecchia and Trombino (2021) and Stoops et al. (2010).

2.3. Electric resistivity tomography

To assess the spatial continuity and homogeneity of the pedogenic horizons and morphologic structures inside the blockstream, we acquired two approximately perpendicular electrical resistivity tomography (ERT) sections upslope the roadcut (Fig. 1b). Each electrical line was acquired with 48 electrodes at 0.5 m spacing, due to the limited available space for electrode deployment with sufficient ground coupling conditions and to get high resolution results in the first meters below the slope surface. The total length of each line was consequently 23.5 m. Despite the moisture of the vegetation and shallow soil cover, the line deployment was slowed down by the high contact resistance measured at the electrodes located on the blocky surface. The surrounding of these electrodes was filled with fine wet materials to enable a better coupling with the ground and ensure proper current flow. The electrode positions were georeferenced using a Garmin GPS60 system, to include the topography of each line in the inversion scheme; the accuracy was 3 to 10 cm. Measurements were acquired through a multichannel resistivity meter (Syscal Pro – Iris Instruments). The acquisition sequence included 545 Wenner-Schlumberger quadrupole configurations along each line. For each quadrupole, measurements were repeated from 5 to 10 times, to reach a standard deviation of the average measured values lower than 5 %. Raw data were then filtered basing on their final standard deviation, measurements showing standard deviation higher than 2 % were finally rejected. The cleaned dataset was inverted in Res2DInv software to obtain two electrical resistivity sections inside the slope.

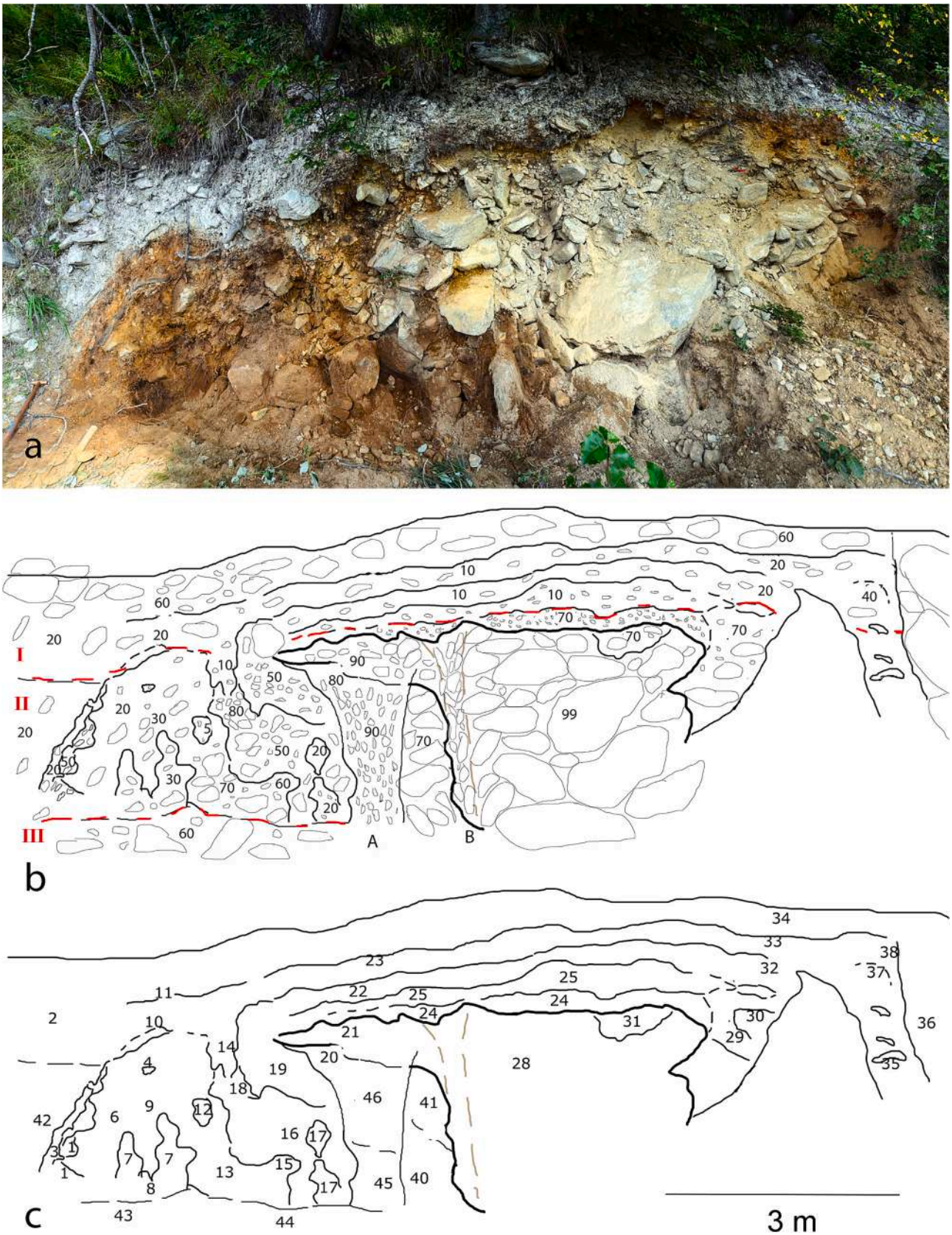

Fig. 2. a: soil profile morphology and internal structure of the studied inter-blockstream transect; b: the stone content (%) is indicated, as well as the major orientation of clasts in the different horizons; the three main structural discontinuities are named in roman numbers (I, II, III), separated by two broken red lines; c: horizon numbers.

3. Results

3.1. Geomorphology and internal structure of the blockstream/inter-blockstream transect

The soil transect showed huge, meters-wide convolutions and injections of different materials (Fig. 2a). The outer limits were open-work stony sectors (blockstreams), only partly vegetated. Their thickness was up to more than 3 m, and their base was not reached. These blockstreams were composed of rounded to subangular coarse stones (0.3–1.5 m), whose size decreased with depth. On the surface they were imbricated and covered with lichens. Their weathering degree was variable, from highly weathered, with thick brownish weathering rinds and easily breakable with a hammer, or even with the hand, to weakly weathered. Many subsurface clasts had a reddish-brown weathering rind and a more angular shape, but still a varied weathering degree.

The central, forested part of the blockstream and inter-blockstream pattern was dominated by fines, but still it was almost completely covered by a shallow stone layer, partly hidden by plants, litter with different decomposition degrees (Oi, Oe and Oa horizons) and mosses. Below the surface layer, the stone content in the fine-dominated soil horizons was varied (Fig. 2b); the weathering degree varied as well, with many horizons characterized by extremely strong stone weathering while others much less (Table 1). There was no regular depth trend of the weathering degree, evidencing mixing of the materials. In the upper horizons (A, E, Bhs and Bhsm horizons), the coarse stones were oriented parallel to the slope, evidencing solifluction or gelifluction. In the central, open course dome-like C horizon, stone fragments were angular and mostly weakly weathered.

Two sectors of the transect could be interpreted as stone-filled wedge-like pseudomorphs, evidenced by letters A and B in Fig. 2b. The left one (A), located inside Bhs, Bs and Bsm sector (horizons n. 45, 46 in Fig. 2c), had an overall finer granulometry (finer clasts) and a looser consistence compared to the embedding materials; the stone fragments were mostly verticalized. The most central wedge (B), surrounded by coarse C materials, was also characterized by an overall vertical orientation and smaller dimension of stones compared to the embedding materials. The coarse infilling of both wedge-like structures probably derived from the collapse of their walls. The lower limit of both structures was not reached, while the upper one was located below the cemented Bsm(v) horizon (horizon n. 24, Fig. 2c).

3.2. Soil characteristics

The soil, classified as Akroskeletic Albic Ortsteinic Podzol (Loamic, Densic, Hyperspodic, Relicticturbic) was complex, showing three structural layers separated by sharp discontinuities. The surface layer (I in Fig. 2b) was a podzolic soil with 30–60 cm thick AE (n. 34) and E horizons (n. 11, 10, 23, 33) above loose dark Bhs ones (n. 22, 32). The E horizons had an abundant vesicular macroporosity (Fig. 3a). Below the loose Bhs, at a depth of around 100–110 cm, a cemented, dense Bsm horizon was visible (n. 25, Fig. 3b), characterized by a coarse platy structure (Fig. 3c).

At the lower boundary of this horizon, layer II started with a very porous, strongly cemented, 10–15 cm thick Bsm(v) horizon, characterized by ca. 20 % of 1–3 mm Fe-Mn nodules sometimes developed inside vesicular pores (n. 24, Fig. 3d). This Bsm(v) horizon separated the podzolic surface layer (I) from the loose, "diapire-like" C horizon composed of large stones and voids (n. 28, Fig. 2c).

Moving towards the blockstreams, below layer I and at the same depth as the C (horizon n. 28), Bhs/Bsm horizons (n. 4, 7, 8, 9, 12, 13, 16, 17, 18) belonging to layer II were present. These horizons showed dislocated and chaotically assembled blocks of cemented horizons, mixed with loose Bs and E portions (Fig. 3e) and blocky aggregates. Below these horizons, the discontinuity with layer III was located at around 270 cm from the surface. This deep layer included cemented, but broken Bhsm horizons (n. 43, 44) that were not mixed with other soil materials; their lower boundary was not reached.

Closer to the limits of lateral stone accumulations on the left, a well-developed Podzol was observed, with thick E horizons (n. 2, 42 in Fig. 2c to a depth of more than 2.5 m) laterally bordering strongly cemented ortstein horizons (n. 1, 6, 9). Below ca. 1 m, the boundary between layer I and II separated the surface E horizon (n. 2) from the E(x) below (number 42), which was extremely compact, brittle and had a coarse platy structure. In addition to high density and brittleness, this horizon shared with fragipans also the fast slaking of the aggregates in water. In nearby roadcuts, this compacted layer formed the bottom of a few streambeds and seepage springs. The colours of some Bs, Bhs and Bhsm horizons were reddish purple (5YR or 2.5YR), particularly around the upper edge of the "diapire-like" C horizon (horizons number 19, 20, 29, 30, 31, 35, Fig. 3f, g, h).

Similarly to the variable weathering degree of the stone fraction, the texture was very diverse in the different horizons, with silt and coarse sand showing the highest and the lowest contents in E horizons and in deep Bhs ones respectively (Fig. 4b, c). Silt caps were abundant mostly in surface layers, otherwise they were visible only in compact E(x) materials. They were absent in disturbed, fragmented subsurface Bs/Bhs/Bsm horizons, inside wedge-like pseudomorphs, and in the central C horizon.

The total organic carbon distribution (TOC, Table 2) was irregular with depth, with particularly high values in some Bhs/Bhsm horizons (up to 6 %). The TOC content in the deepest Bhsm (numbers 43, 44) horizons was particularly high (4.5——5.0 %). Some rootlets were covered with well-cemented purple materials in horizons 20 (Fig. 3i), 43 and 44, likely ascribable to Fe-SOM associations, as suggested by the high TOC contents in these horizons.

Fe and Al forms showed a strong redistribution due to podzolization processes (Table 2). The Feo/Fed ratio was high in some horizons, particularly in the organic matter-richest Bhs-Bhsm horizons. Very high Feo, Alo and TOC contents were also observed in very deep horizons, located also below cemented layers.

3.3. Clay mineralogy

The different clay mineral assemblages in the different horizon types confirmed the strong podzolic pedogenesis (Table 3). In particular, the analyzed E horizons (n. 2, 23, 36), likely active at present, were rich in illite–smectite interlayered minerals (rectorite), characterized by very sharp peaks at ca. 2.4 nm and shifting to ca. 2.7 nm after EG solvation, suggesting a regular mixed-layer mineral (Fig. S1a). The lateral Bs (n. 6) had appreciable quantities of this mineral as well. Illite-vermiculite interlayered minerals were observed in all the analyzed soil horizons (peak at ca. 2.4 nm upon Mg-saturation, no swelling after EG solvation and shifting to ca. 2.0 nm after heating at 350 °C), without clear differences in different horizon types. Vermiculite (peak at around 1.42 nm shifting to ca. 1.0 nm after heating) was observed only in some Bs, Bhsm, Bm(v) and C horizons (n. 22, 24, 28, 44, Fig. S1b, S1c, S1e), while chlorite was detected in substantial amount only in horizons n. 6 and 25 (in 22, 24 and 28 in traces, Fig. S1c and S1d). Kaolinite was observed in all samples, with the lowest content in E horizons. Gibbsite (peak at 0.48 nm) was observed in many spodic and C horizons (n. 6, 22, 24, 25, 28, 44, Fig. S1b, S1c, S1d, S1e). The deepest Bs horizon (horizon n. 44) had the highest content of gibbsite. Lepidocrocite (peak at 0.63 nm) was observed in some Bs horizons (horizons 6, 22, 44, Table 3). The Bsm(v) and the central C horizons (24 and 28) were similar to spodic horizons, showing relatively large kaolinite and vermiculite contents, and traces of gibbsite and chlorite.

The pH_{NaF} values (Table 2) evidenced large ITMs contents in most Bs/Bhs/Bhsm horizons, with particularly high values in purple and in cemented ones, irrespective of depth. These minerals were not detected in the E horizon.

Table 1
Morphological properties of the soil horizons; the first column corresponds to horizon numbers in Fig. 2c. Cells are empty when the property was lacking.

Layer	Hor. number	Horizon type	Colour	Mottles	Roots	Primary structural aggregation	Consistence	Stone weathering stage	Silt caps (SC), vesicles
I	11	E	10YR 6/3	N	F, FI-CO	SS	Loose	S-M mixed	SC Common, thick
I	34	EA	10YR 4/2	N	F, FI-CO	S, PL, ME	Loose	F	SC fine and soft
I	23	E	10YR 6/4	N	F, FI	S, PL, ME	Hard	S	SC thick and hard
I	33	E	10YR 7/2	N	F, FI-CO	S, PL, ME	Compacted, friable	M	N
I	10	E	2.5Y 7/2	N	F, FI-CO	S, PL, ME	Compact, friable	S	SC Common, medium
I	2	E	10YR 7/2	N	F, FI-ME	M, PL, ME	Compacted, hard	S	SC Many, thick
I	38	E	10YR 7/2	N	F, FI	W, PL, CO	Friable	F	N
I	36	E	10YR 5/4	N	F, FI	S, PL, ME	Loose	F-M	N
I	37	BE	10YR 5/6	N	N	W, PL, ME	Soft	S	Thick SC
I	32	Bhs	10YR 3/6	N	N	W, SB, FI	Friable	S	N
I	22	Bs/Bsh	7.5YR 5/8	N	N	S, SB, ME	Friable	F	SC thick and hard
I	25	Bsm	7.5YR 5/8	10YR 6/6	F, FI-CO	S, SB, ME	Compacted and moderately cemented	M	SC thick and hard
II	24	Bsm(v)	2.5Y 5/6	N	N	S, PL, FI	Strongly cemented	F	Vesicles, some filled with Fe-Mn nodules
II	42	E(x)	10YR 7/3	N	N	S, PL, CO	Compacted, very hard	S	N
II	3	EB(x)	10YR 6/4	N	N	S, PL, CO	Compacted, very hard	S	N
II	1	Bsm	7.5YR 5/8	N	C, FI-ME	S, SB, ME	Compacted, hard	M	N
II	4	EB	10YR 6/6	N	F, FI	M, PL, ME	Friable	S	SC Few, fine
II	5	Bs	7.5YR 5/7	N	N	W, SB, ME	Loose	M	N
II	6	Bs	8.5YR 6/8	N	N	W, SB, ME	Loose	S	N
II	9	Bs/Bh	Mixed	N	A, FI-CO	SS	Loose	F-S mixed	N
II	12	Bhs	5YR 4/4	10YR 6/3	C, FI	SS	Loose	S	N
II	7	E/Bs/Bhs@	Mixed	N	F, FI	W, SB, ME	Loose	M	N
II	8	Bhs	5YR 3/4	N	N	W, SB, ME	Friable	M	N
II	13	Bhs	7.5YR 5/8	N	A, FI-CO	W, SB, ME	Very friable	M	SC, Common thin
II	15	Bhs	7.5YR 3/3	N	A, FI-CO	W, SB, ME	Loose	F-S mixed	N
II	14	E	10YR 7/3	N	N	S, PL, ME	Hard	S	Vesicles
II	18	E@/Bhs@	7.5YR 3/4	N	N	SS	Loose	F-M mixed	N
II	16	E(/Bs/Bhs)@	10YR 6/4	7,5YR 4/3	N	M, PL, FI	Friable	S	SC thick and hard
II	17	Bs/Bsh/Bhs	7.5YR 3/4	5YR 4/6	N	S, SB, ME	Friable/cemented	M–S mixed	N
II	19	Bs/Bhs	7.5YR 3/4	5YR 4/6	N	W, SB, ME	Loose	F	N
II	30	Bsh	2.5YR 2.5/2	N	N	W, SB, ME	Loose	M	SC fine and soft
II	29	Bs	2.5YR 2.5/4	N	N	W, SB, ME	Loose	M	SC fine and soft
II	31	Bsm	2.5YR 4/6	7.5YR 5/8	N	S, SB, CO	Strongly cemented	F	N
II	35	Bhs	5YR 3/6	N	N	W, PL, ME	Loose	M	SC coarse
II	26	Bsh@/Bs@	7.5YR 3/4	N	N	W, SB, ME	Friable/loose	S-M	N
II	27	Bs	7.%YR 5/8	N	F, FI	W, SB, ME	Loose	M	N
II	20	Bhs(m)	5YR 3/4	N	N	S, SB, CO	Weakly cemented	M	N
II	21	Bhsm	5YR 3/3	N	N	S, PL, CO	Strongly cemented	M	SC thick and hard
II	28	C@	2.5Y 5/7	N	N	SS	Loose	F	N

(*continued on next page*)

Table 1 (*continued*)

Layer	Hor. number	Horizon type	Colour	Mottles	Roots	Primary structural aggregation	Consistence	Stone weathering stage	Silt caps (SC), vesicles
II	40	Bsh/Bshm@ mixed randomly	5YR 4/8	N	N	S, SB, ME	Loose	F-S	N
II	41	Bs	7.5YR 6/8	N	F, FI	S, SB, ME	Loose	M–S–F	N
II	45	Bs	7.5YR 4/8	N	N	S, SB, ME	Loose	F-M	N
II	46	CB	10YR 5/8	N	N	SS	Loose	F	N
III	43	Bhsm	5YR 3/6	N	N	S, BS, CO	Cemented but broken	F-M	Broken and mixed
III	44	Bhsm	5YR 3/5	N	N	S, BS, CO	Cemented but broken	F-M	Broken and mixed

Abbreviations (IUSS Working Group WRB, 2022):
Roots quantity: abundant (A), common (C), few (F), none (N); roots dimension: fine (FI), medium (ME), coarse (CO).
Grade of structure: weak (W), medium (M), strong (S); type of structure: single grain (SS), subangular blocky (SB), platy (PL); size of aggregates: fine (FI), medium (ME), coarse (CO).
Stone weathering degree: strong (S), moderate (M), fresh material (F).

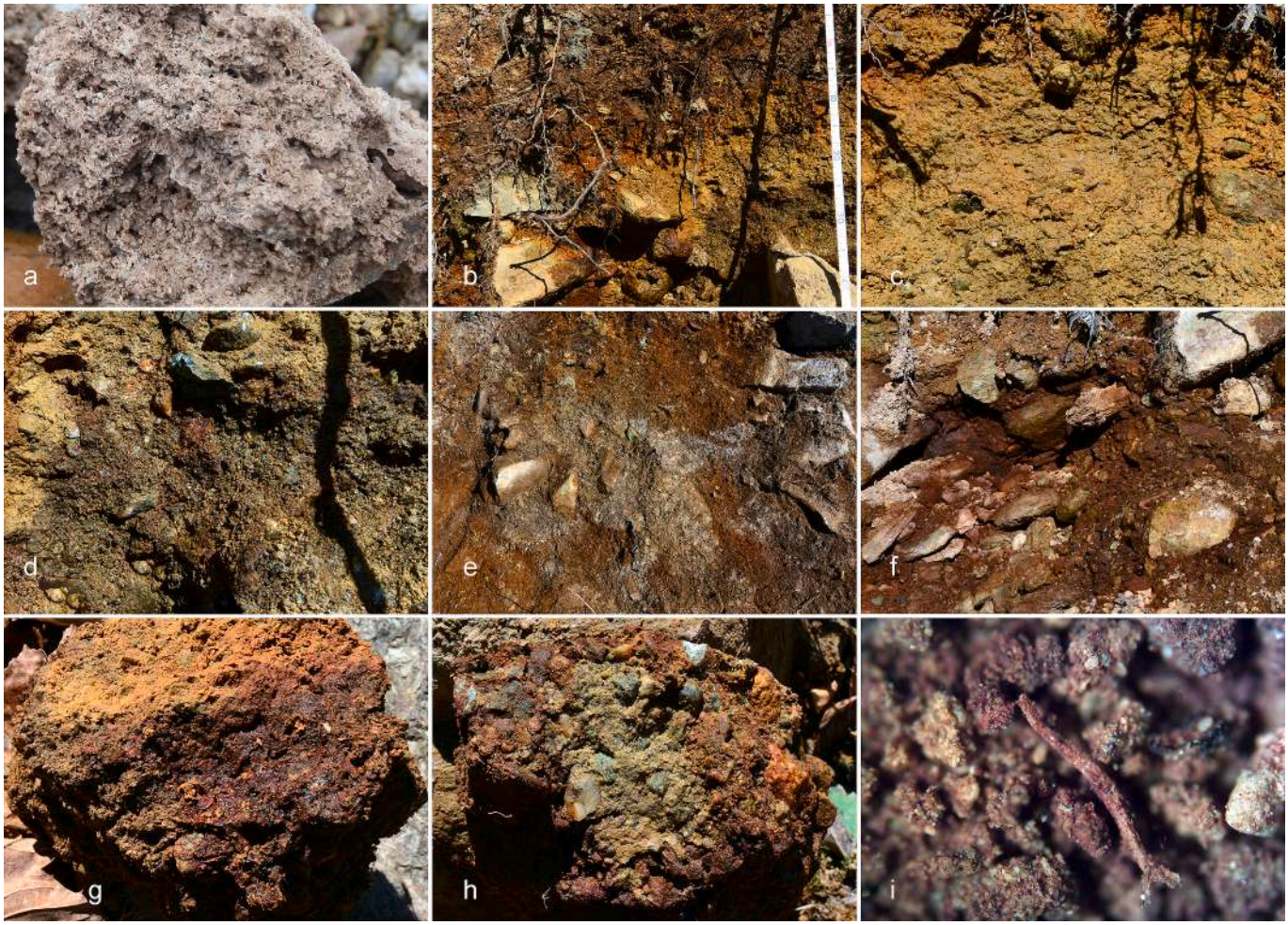

Fig. 3. A: bhs, bsm and Bsm(v)/Bhsm sequence on the left of the C horizon inclusion (horizons number 22, 25, 24, 20, 21); b: purple-coloured horizons number 21, 20 and 19; c, e: cemented aggregates from horizons number 21 and 19; d: rootlet covered with purple Fe-SOM compounds in horizon 20; f: abundant fine black Fe-Mn nodules in the Bsm(v) horizon (n. 24).

3.4. Micromorphology of the Bsm(v) horizon

The strongly cemented Bsm(v) horizon (number 24) showed many dark Fe-Mn impregnative pedofeatures (Fig. 5A-b, 5B-b, 5D-b and Fig. 5F-b), in addition to the many nodules observed in the field. These pedofeatures often cemented silt coatings around stone fragments or cracks and pores (Fig. 5B-c, 5D-c, 5F-c); layering was not evident, suggesting that they might have developed during a single pedogenic phase. Some pores were coated by yellowish brown or dark brown spongy coatings (Fig. 5A-a), typical of spodic materials (Verrecchia and Trombino 2021). Some pores were also filled with layered, rather limpid orange clay coatings (Fig. 5E-e, 5F-e), which showed many angular

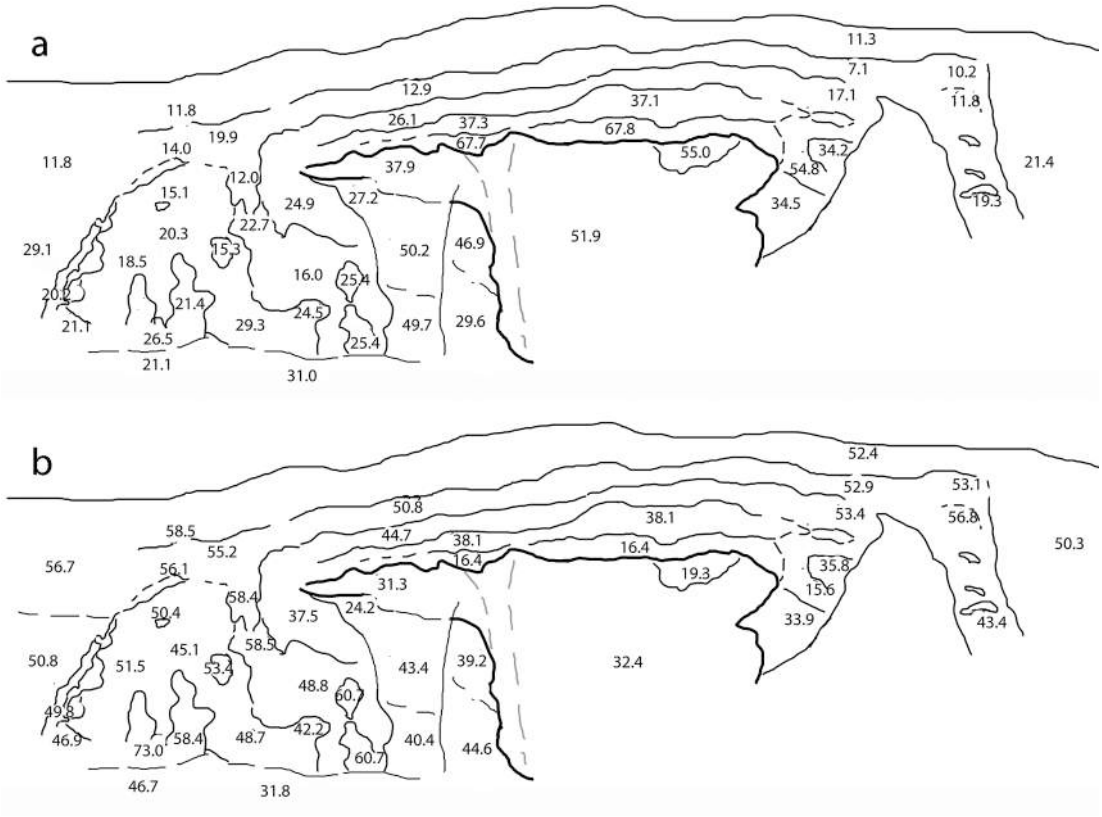

Fig. 4. Contents of a: coarse sand (%); b: silt (%) in the different soil horizons.

cracks (Fig. 5C-d, 5D-d).

3.5. Geophysical investigations

The ERT sections showed high lateral and vertical heterogeneity in the investigated transect (Fig. 6). The electrical resistivity values were in general very high (> 10 kOhm m). The only low resistivity part of each section was in the first 30 to 50 cm of depth, coherently with the presence of the fine-grained soil horizons, moist at the time of the investigation. Below this depth, high resistivity values were often observed, with clear lateral variations. The higher resistivity zone found along L1 (> 70 kOhm m) partly corresponded to the open-work, "diapire-like" C horizon observed in the central part of the transect. These extremely high values were consistent with the presence of dry and coarse-grained stony materials with high porosity and confirmed the continuation of the structure along the slope. Similar materials were found in the cross-cutting L2, also at higher elevations, in the central part of the section. The lateral variations in electrical resistivity at these depths were well explained by the variation in the stone content shown in Fig. 2b for the transect. The unweathered bedrock below the slope materials was not reached.

4. Discussion

4.1. Age and genesis of landforms and soils

The internal structure and the materials composing the observed 3 m-thick section (blockstream –vegetated central part – blockstream) suggest many different processes active during long periods across the Quaternary, pointing to a strong polygenesis of both soils and landforms. Their good preservation and their particularly strong development can also provide important information on the forming processes of such periglacial features in mountain slopes. In fact, as in the Bric Mindino slope, blockstreams are often arranged as large-scale sorted stripes (Rixhon and Demoulin, 2013), particularly where no cliffs lie above the block accumulations (van Steijn et al., 2002). 1–15 m wide vegetated stripes (sorted stripes) between blockstreams are characteristic of the Falkland Stone Runs (André et al., 2008), while similarly coarse but unsorted stripes are preserved in England (Ballantyne and Harris, 1994). The absence of source rock faces above the blockstreams/blockslopes on Bric Mindino is one of the proofs of the particularly old age of the landforms, as the rock face, source of the blocks, has been completely destroyed by long-lasting cryofracturation processes (e.g. Paro, 2011).

The different weathering degree of the stones in the blockstream and in some soil horizons (together with other weathering indicators, such as texture and clay mineralogy) suggests different periods of activity and exposition to surface and/or pedogenic processes. This implies an overall old age of the landforms, shaped during many different Quaternary glacial-interglacial phases, as reported by other studies in the unglaciated Ligurian Alps (Rellini et al., 2014; D'Amico et al., 2016, D'Amico et al., 2019), or in the Sudetes and elsewhere (summarized by Engel et al., 2020). The rounded or subrounded shape and the thick weathering rinds on many stones in the stone stripes point to a long-term exposure at the surface or at shallow depths. Indeed, stone accumulations on the mountain tops (the so-called mountain top detritus, also known as blockfields, often grading into blockstreams on nearby slopes) have been sometimes interpreted as developed across long periods during or even before the Pleistocene (Ballantyne, 1998; Andrè et al., 2008).

Our deep soil profile allowed us to likely find very old soil layers (pre-MIS4), such as the Bs/Bhsm/E horizons, mixed probably by deep cryoturbation processes (differential frost heave) or load casting during permafrost degradation (Van Vliet-Lanoë, 1991a), active after their formation (layer II). The deep, fragmented Bhsm (43, 44) was also likely broken by ice formation in a permafrost environment (layer III). These evidences suggest that present day soils (Podzols) in the uppermost part

Table 2
TOC, pH_{NaF}, Fe and Al data and the Spodicity Index (SI, Alo + 0.5*Feo, %) in the main pedogenic horizons. Oxalate and dithionite extractable elements were analyzed only in some characteristic horizons.

	Horizon type	pH H_2O	TOC %	Feo g kg^{-1}	Alo g kg^{-1}	Fed g kg^{-1}	SI %	pH NaF	Feo/Fed
11	E	3.7	0.96	NA	NA	NA	NA	7.0	NA
34	EA	4.1	2.88	0.48	1.95	2.01	0.22	7.0	0.25
23	E	3.8	0.59	0.40	1.47	2.31	0.17	7.0	0.17
33	E	3.7	0.84	NA	NA	NA	NA	7.0	NA
10	E	3.8	0.43	NA	NA	NA	NA	7.0	NA
2	E	3.8	0.44	0.26	1.72	1.78	0.19	7.0	0.14
38	E	3.8	0.71	NA	NA	NA	NA	7.0	NA
36	E	3.7	1.17	NA	NA	NA	NA	7.0	NA
37	BE	4.0	1.43	NA	NA	NA	NA	7.0	NA
32	Bhs	4.3	3.29	NA	NA	NA	NA	9.0	NA
22	Bs/Bsh	4.4	1.31	11.76	3.90	13.76	0.98	9.0	0.86
25	Bsm	4.9	0.68	2.05	4.81	5.78	0.58	11.5	0.36
24	Bsm(v)	5.0	0.98	0.88	12.21	4.36	1.27	8.5	0.21
42	E(x)	4.2	0.38	0.58	1.36	2.39	0.16	7.0	0.25
3	EB(x)	4.1	0.72	NA	NA	NA	NA	7.0	NA
1	Bsm	5.4	1.19	NA	NA	NA	NA	9.0	NA
4	EB	4.3	1.03	NA	NA	NA	NA	7.0	NA
5	Bs	4.7	1.12	NA	NA	NA	NA	9.0	NA
6	Bs	4.7	1.27	11.86	4.24	13.99	1.02	9.0	0.85
9	Bs/Bh	4.7	2.72	9.36	5.22	12.13	0.99	9.0	0.77
12	Bhs	4.7	2.71	NA	NA	NA	NA	8.5	NA
7	E/Bs/Bhs@	5.2	2.7	NA	NA	NA	NA	9.5	NA
8	Bhs	5.1	2.9	NA	NA	NA	NA	11.5	NA
13	Bhs	5.0	3.39	NA	NA	NA	NA	11.5	NA
15	Bhs	5.0	3.09	NA	NA	NA	NA	11.5	NA
14	E	4.1	0.75	NA	NA	NA	NA	7.0	NA
18	Mixed	4.3	3.27	15.98	7.58	18.37	1.56	11.5	0.87
16	E(/Bs/Bhs)@	4.5	0.9	NA	NA	NA	NA	7.0	NA
17	Bs/Bsh/Bhs	5.1	3.11	15.72	7.71	17.7	1.56	9.5	0.89
19	Bs/Bhs	4.9	3.69	18.19	14.26	19.12	2.34	11.5	0.95
30	Bsh	4.9	9.28	6.36	20.52	9.06	2.37	11.5	0.71
29	Bs	4.9	7.21	5.98	27.92	8.01	3.09	11.5	0.75
31	Bsm	5.1	3	NA	NA	NA	NA	12.0	NA
35	Bhs	4.8	4.12	NA	NA	NA	NA	10.0	NA
26	Bsh/Bs/mixed	4.9	3.21	9.49	6.51	11.71	1.13	10.0	0.81
27	Bs	5.0	1.98	10.58	8.68	13.08	1.40	11.0	0.81
20	Bhs(m)	5.1	7.95	NA	NA	NA	NA	10.0	NA
21	Bhsm	5.0	5.6	26.73	25.36	27.07	3.87	11.5	0.99
28	C@	5.6	0.69	1.24	6.15	4.89	0.68	10.5	0.25
40	E/Bsh/Bshm@	5.0	3.1	13.84	8.57	16.24	1.55	11.0	0.85
41	Bs	5.2	1.13	NA	NA	NA	NA	10.0	NA
45	Bs	5.7	4.35	23.97	17.50	24.64	2.95	11.0	0.97
46	CB	5.1	6.5	NA	NA	NA	NA	11.0	NA
43	Bhsm	5.8	5.03	6.32	7.43	8.52	1.06	11.5	0.74
44	Bhsm	5.8	4.54	25.77	15.43	26.91	2.83	11.5	0.96

NA: not analyzed.

Table 3
Semiquantitative clay mineralogy of some characteristic horizons. Cells are empty when the mineral was not observed in the sample. Symbols: xxx = abundant; xx = common; x = scarce; – = trace.

	Quartz	Lepid.	Goeth	Kao	Gibbs	Chl	IV	IS	Verm	Illite
2 – E	x			x			xx	xxx		X
6 – Bs	x	–	–	x	–	x	xxx	X		x
22 – Bhs	x	–	–	xx	–	–	xxx		x	X
23 – E	x			x		–	xxx	xxx		x
24 – Bsm(v)	x			xx	–	–	xx		xx	Xx
25 – Bhsm	x			xx	–	x	xx			xx
28 – C@	x			xx	x	–	xxx		xx	x
36 – E	–			xx			xx	xxx		Xx
44 – Bhsm	x	x		x	x		xx	x	xx	x

Lepid: lepidocrocite; Goeth: goethite; Kao: kaolinite; Gibbs: gibbsite; Chl: chlorite; IV: illite-vermiculite interlayered minerals; IS: illite–smectite intelerayered minerals; Verm: vermiculite.

of the transect (Sector I), were the "climax" soil type also in most previous interglacial periods.

The extremely thick E horizons close to the stony borders, which includes a deep layer (E(x) horizon in sector II) visibly influenced by ice-lensing in a permafrost environment, is another indicator of pre-LGM pedogenesis.

The clay mineralogy of the 3 m-deep Bhs/Bhsm horizons (layer III) showed a much higher weathering degree than the upper layers II and I, with quite large quantities of gibbsite, pointing to a particularly old age as well, and different weathering environments. In fact, gibbsite and

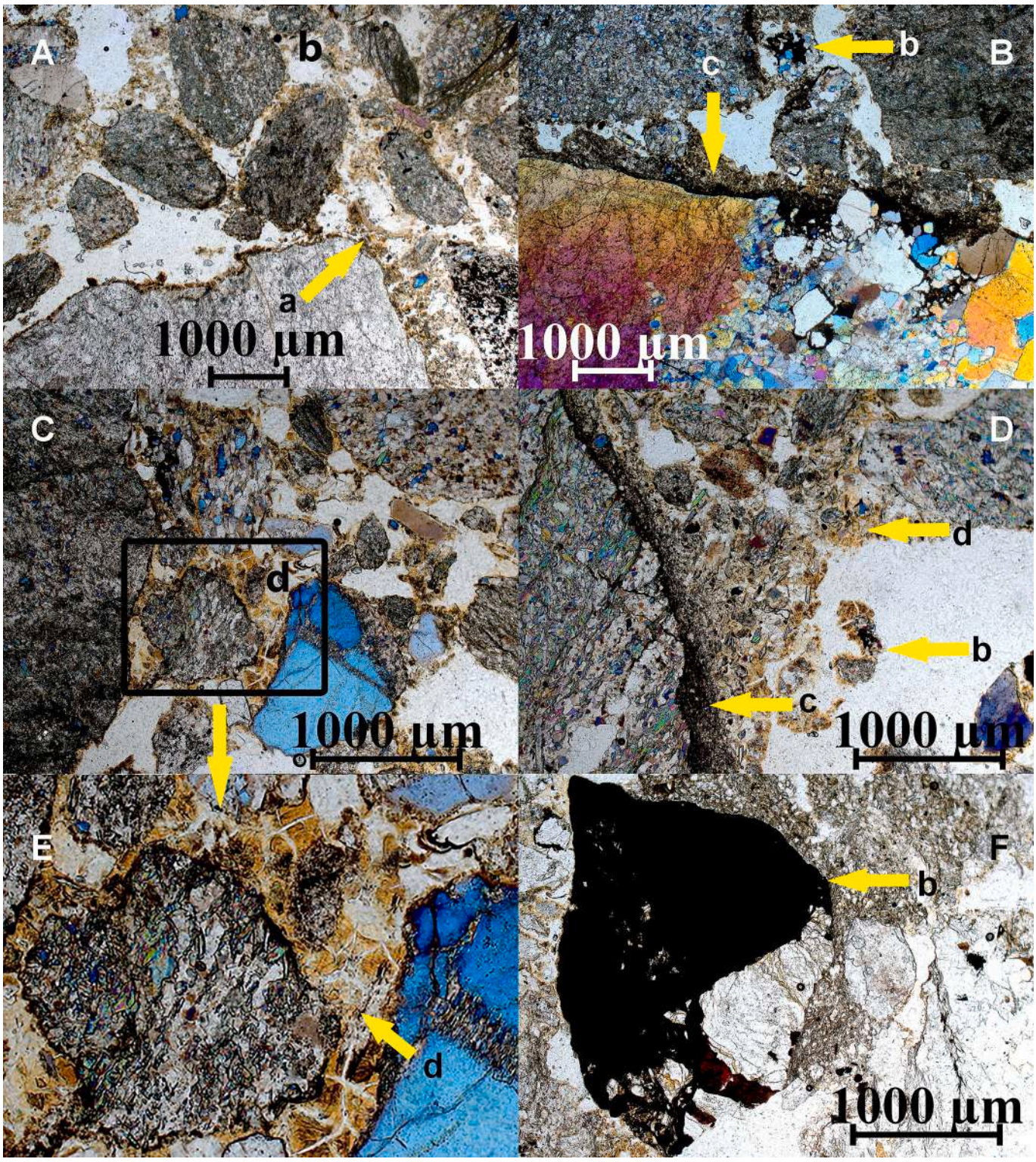

Fig. 5. Micromorphlogical features from the Bsm(v) horizon (small letters with arrows): a – spongy cracked coatings typical of spodic materials (in Fig. 5A); b – Mn-coloured Fe-Mn-masses and nodules (in Fig. 5B, 5D, 5F); c – silty accumulations, cemented by Fe and Mn, coloured by black Mn oxides (in Fig. 5B, 5D); d – finely layered, deeply cracked clay coatings (in Fig. 5C, 5D, 5E).

kaolinite need long times for formation but not necessarily subtropical climatic conditions (Goodfellow et al., 2014). In Northwestern Europe, gibbsite is typically found in soils located above the glacial trimline (i.e., which escaped glacial erosion during the LGM, Ballantyne et al., 2007); it can thus be considered an indicator of old age.

Old age and deep weathering can also be assumed from the central C horizons (n. 28): despite the low clay fraction content (ca. 7 % of 1–2 % total fine earth), the lack of structural aggregation and the weak and pale pigmentation, its mineral composition is dominated by pedogenic clays and not by primary minerals.

Given the high pedogenic development degree highlighted by the above-mentioned data, the indications of pre-MIS4 pedogenesis, the

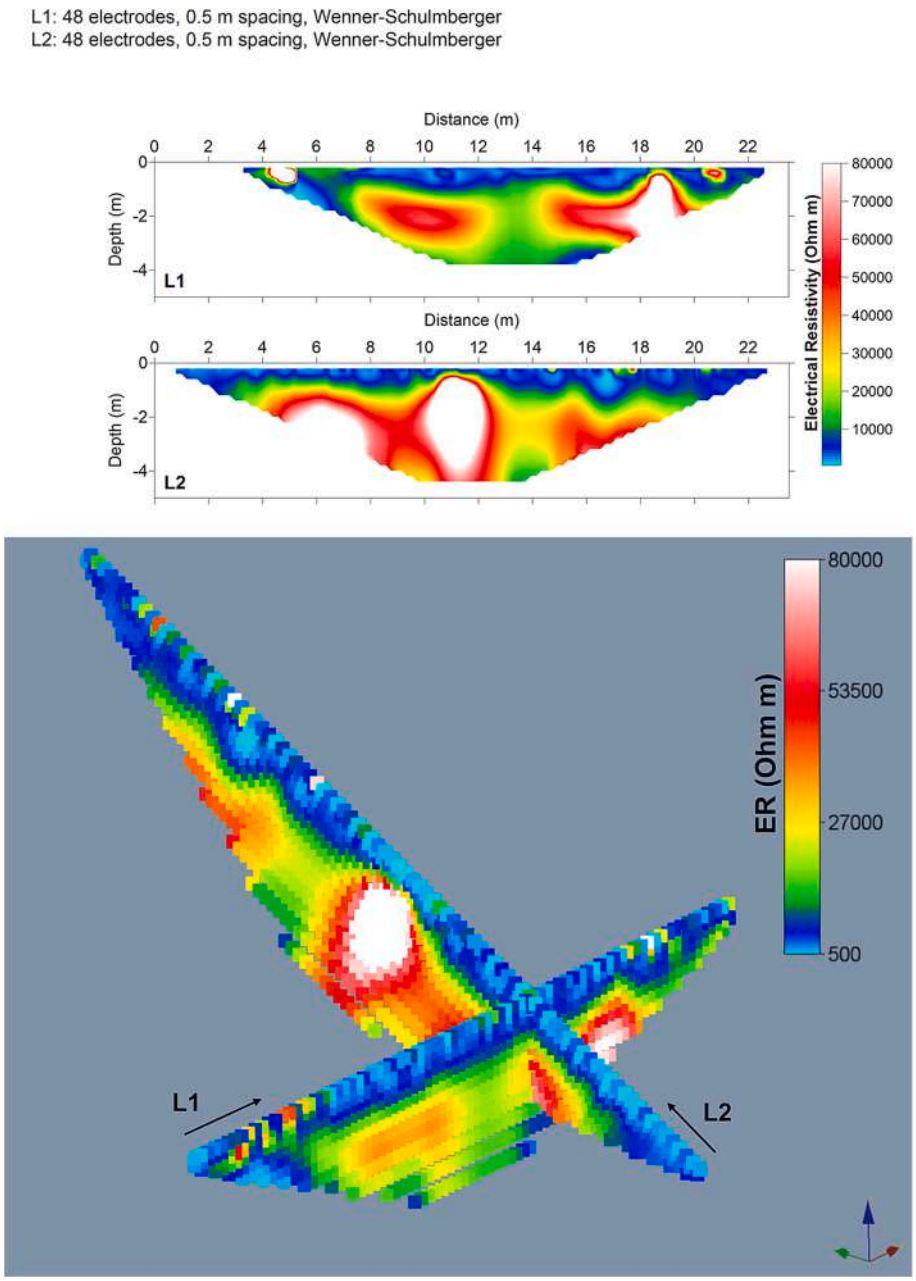

Fig. 6. Electrical resistivity tomography results: L1, perpendicular to the slope and nearly parallel to the road cut (a) and L2, parallel to the slope (b). (c) 3D reconstruction of the geometry and intersection of the ERT sections.

many different discontinuities observed in palesosols nearby (D'Amico et al., 2016; 2019), and the different stone weathering degree, we can hypothesise a similar age to the Falkland stone runs (at least 700–800 ka, according to Wilson et al., 2008). The Scottish mountain top detritus (blockfields and blockstreams) also developed through long periods and at least part of the weathering took place apparently before the Quaternary (Hall et al., 2019).

4.2. Paleoclimatic interpretation

Blockstreams, without an impermeable rock layer below, are indicators of permafrost conditions (e.g. Wilson et al., 2017). At the elevation of the studied soil profile (1460 m a.s.l.), permafrost probably disappeared not much later after the end of the LGM, as the terminus of rock glaciers, proxy of the lowest elevation of discontinuous permafrost, during the Egesen stadial (aka Younger Dryas) was at elevations higher than 1800 m a.s.l. in the Alps (e.g., Federici et al., 2008; Scotti et al., 2013). The stone concentration in the lateral blockstreams and in the upmost horizon in our section indicates intense frost sorting, both laterally and vertically (Traczyk and Migoń, 2000). The downslope alignment of stones in the upper layers is evidence of solifluction or gelifluction above a shallow permafrost table. In addition, many other cold climate and permafrost indicators are however detectable in the soil section, such as traces of many processes associated to ice lensing and surface freeze–thaw activity during cold periods, confirming the alternating climatic conditions that have succeeded during soil and landform development (Table 4).

The abrupt change of many structural and morphological properties at the boundary between layer I and II, and then III, suggests the presence of a permafrost table at around 1–1.2 m depth for long periods, and a deeper one at ca. 2.80 m. This was already hypothesized in other paleosols in the area (D'Amico et al., 2019). In particular, impermeable

Table 4
Geomorphic, pedogenic and mineralogical evidences and paleoenvironmental indications.

Relict feature	Process	Horizon numbers	Paleoenvironmental indications	Ref.
Blockstreams	Gelifluction	36; lateral blockstreams	MAAT < −6°C, permafrost in absence of hard rocky substrate	Harris (1994);Karte (1983); Murton (2007); Wilson (2013)
Stones oriented parallel to the slope	Solifluction/gelifluction	2, 10, 11, 22, 23, 25, 32, 33, 34	Intense cold conditions	Müller and Thiemeyer (2014)
Stone concentration in the soil surface and with decreasing stone diameter with depth	Frost sorting	34, 23, 36, Lateral blockstreams	Intense cold conditions	Traczyk and Migoń (2000)
Mixing of soil materials derived from different Bhsm, Bsm, Bs and E horizons	Cryoturbation	4, 7, 8, 9, 12, 13, 16, 17, 18, 2	Intense cold conditions	Bockheim and Tarnocai (1998)
Hard layer with platy structure	Thaw unconformity – Permafrost table at 80–120 cm;	24, E(x)	Permafrost conditions (MAAT < −3°C)	Van Vliet-Lanoë (1998); French and Shur (2010)
Vesicular pores	High air/water pressure during fast freezing	19, 24, 25, 29, 30	Fast freezing in the active layer, high pressure because of impermeable frost below	Hamilton (1977); Skvortsova et al. (2020)
Fe-Mn nodules filling former vesicular voids	Thaw unconformity – Permafrost table at 80–120 cm; transient layer	24	Permafrost conditions (MAAT < −3°C)	Jacobsen et al., (1996); Sedov et al. (2016); Vogt and Larquè (2002); van Vliet-Lanoë (1991b)
Broken Bhsm horizon below the cryogenic involutions	Thaw unconformity – Permafrost table at 3 *m*	43, 44	Permafrost conditions (MAAT < −3°C)	Watson and Morgan (1977)
Large-scale involutions, higher than 2 *m*	Load casting, Thermokarst in ice-rich permafrost bodies		Ice-rich permafrost, MAAT < -6	French et al. (2005); Karte (1983); Vandenberghe et al. (2016)
Open-work structure of stony materials	Presence of ice lensing/ice bodies	42, 21, 28	Permafrost conditions (MAAT < −3°C)	Van Vliet-Lanoe (1998); French and Shur (2010)
Sections with oriented, rather well graded stones in two wedge-like structures	Stony wedge pseudomorphs	45, 46	Permafrost, particularly harsh winters; MAAT < -8°C, or < -6°C	Murton et al. (2000); Murton (2007); Romanovskii (1985); Merrits and Rahnis (2022)
Silt coatings on stones	Cryosuction – pervection	2, 11, 16, 21, 22, 23, 24, 25, 35, 37	Intense soil frost, seasonal or permafrost (pervection)	Van Vliet-Lanoe (1998); Frenot et al. (1995)
Strongly developed E, Bhs, Bs and Bsm horizons; spongy coatings in thin section.	Podzolization	Most	Well-developed vegetation cover, quite high rainfall, cool temperatures	Lundström et al. (2000)
Gibbsite	Long lasting weathering	6, 22, 24, 25, 28, 44	From temperate to tropical conditions	Ballantyne et al. (2007)
Different weathering degrees of stones	More than one phase of activity of blockstreams, separated by temperate-climate weathering regime	blockstreams, 9, 11, 15, 17, 18, 36, 40	From cold to at least temperate climates	D'Amico et al., (2019)
Fragmentation of clay coatings	Cryoturbation, ice lensing (if no smectitic components are present)	24	Cold condition/permafrost	Cerbian et al.,(2020)
Clay coatings	Clay illuviation	24	Temperate, humid forest	Schaetzl and Anderson (2015)

horizons with coarse platy aggregation (E(x) and Bsm(v) horizons) and fragipan-like layers (E(x)) have often been considered as indicators of an ancient permafrost table (Fitzpatrick, 1956; Van Vliet-Lanoë, 1998), at a rather constant depth (D'Amico et al. 2019, D'Amico et al., 2016). Another indicator of a past permafrost table is the nodular Bsm(v) horizon. In fact, Fe-Mn accumulation have been sometimes observed near the permafrost table in present-day soils (e.g., Jacobsen et al., 1996; Vogt and Larquè, 2002); however, a detailed description of such nodular/cemented horizons is seldom available (do Vale Lopes et al., 2019). Evidence of waterlogging or perched water table in a freely drained soil can be an indicator of past permafrost conditions (van Vliet-Lanoë, 1991b).

The rootlets covered by Fe oxides in deep horizons (43 and 44) could also be a legacy of permafrost conditions, as rootlets and plant remnants are often well preserved inside ice-rich permafrost bodies in Arctic areas (Lupachev and Gubin, 2023).

The "diapire-like" shape of the coarse central part of the vegetated sector, composed of open-work boulders, can suggest particularly cold conditions and ice-rich permafrost. Ice lensing in gravelly materials is often observed (French et al., 2005), and significant ice bodies can occur within coarse sediments (Gowan and Dallimore, 1990), even if they are most common in silty or loamy materials, and they depend on the presence of a sufficient water supply. In Alpine slopes, ice-rich permafrost (filling the voids in the open-coarse materials and with lenses up to 60 cm thickness) is at present normally observed inside periglacial rock glaciers, or frozen talus slopes (Jones et al., 2019). The result of the high ice content would be a suspended cryostructure (French and Shur, 2010), which would be able to explain the large void volume, also detected by ERT. The large ice content would also imply an important swelling of the topographic surface during permafrost periods, able to separate stone stripes and to disrupt and mix previously developed spodic horizons. Particularly large ice contents are expected in the coarse materials at the base and in the central part of the studied section, able to explain its upward expansion at the expense of the more frost-susceptible finer materials in the upper part. In fact, normally, sandy gravels above fine sand facilitates thermokarst involution formation (Sharp, 1942; Van Vliet-Lanoë, 1998). In our slope, the probable ice-rich bodies could be possible thanks to the emergence of rather deep groundwaters, injecting water laterally in the slope (Haeberli and Mühl, 1996; Vandenberghe et al., 2016). The spring waters emerging presently from within the slope near the soil profile could support this hypothesis.

At the time of permafrost degradation, thick ice bodies in the open-work coarse material would require more time for melting compared to the finer materials on its side (because of latent heat of fusion), and this could create differential load casting able to increase the dimensions of the coarse involutions. In fact, involutions deeper than 2 m are usually considered caused by thermokarst and not cryoturbation (French et al., 2005). Similarly large cryoturbation structures, likely due to load casting during ice-rich permafrost degradation, have been described by Vandenberghe et al., (2016) and Harris et al., (2017).

In the Appalachian Mountains, similar large-scale cryogenic structures have sometimes been interpreted as gelifluction sheets during permafrost degradation (Merrits and Rahnis, 2022). Open-work boulder assemblages under 1–2 m of finer soil materials have been observed in LGM periglacial areas in Pennsylvania, but they have been interpreted as buried blockstreams, even if their shape shows a clear upwelling

(Denny, 1956). Upwelling of coarse materials under the central parts of sorted circles have been observed in the Svalbard Islands as well (Kasprzak, 2015). Moreover, other dome-shaped stony structures in the stone-free sectors of large scale sorted stripes have been observed in other roadcuts in unglaciated slopes in the Western Alps by the authors (unpublished). We can thus hypothesise that the described processes associated to ice-rich permafrost in mountain slopes showing large-scale stone stripes and blockstreams might have been common during cold Pleistocene periods.

The ice wedge-like pseudomorphs can be interpreted as both actual ground ice wedge pseudomorphs, or structures associated to differential blockstream movements along the slope. In the first case, they would be pseudomorphs developed inside ice-rich coarse slope materials. Their upper limit would correspond to the permafrost table during the coldest periods, in agreement with the cemented layer above characterized by abundant vesicles partly filled with Fe-Mn nodules. Wedge pseudomorphs with their upper boundary under cemented horizons have also been observed in Patagonia (Vogt, 1992). In that case, the cemented layer was a calcrete, which showed typical cold-climate morphology.

However, wedges in such coarse materials have not been often described. Wedge pseudomorph-like structures filled with stones were described in polygonal patterned ground in the Rocky Mountains by Benedict (1979). The processes responsible for the infilling have not been hypothesized, and no proof of their true fossil ice/soil wedge nature has been given. Pissart (1970) showed stone-filled wedge pseudomorphs in the Arctic, while at present active ice wedges have been observed in coarse talus slopes in Antarctica (Levy et al., 2013). Usually, sand wedges are filled with fine aeolian materials, while the composite wedges shown by Ballantyne and Harris (1994) are filled with material derived from creep and saltation, a mix of locally derived and heterogeneous sediments. Soil wedges are normally smaller, less than 1 m deep and broader (0.3–0.6 cm wide), irregular in form; the infilling is massive and without laminations, and reflect seasonal frost cracks (Murton, 2007). Ice wedges can be seldom filled with stones derived from the collapse of their walls (Murton, 2007), or from collapse/solifluction of the materials above them. In coarse materials, particularly cold conditions are required (MAAT $< -6°C$, Romanovskii, 1985). The sloping position could however have favoured the infilling by stones derived from the collapse of upstream walls of the wedge-like structure. A downward convexity in the Bsm(v) horizon above could be a proof of the actual presence of an ice wedge, later filled with stones.

The presence of well-developed, old soils might seem unlikely in such heavily cryoturbated slopes. However, many paleosols showing evidences of pre-LGM pedogenesis have already been described in the area (D'Amico et al., 2016, 2019). Moreover, some paleosols have been preserved inside permafrost bodies for at least one glacial cycle (but also even many more). For example, Podzols preserved in permafrost layers throughout the LGM have been locally observed in Finland, (Pitkäranta, 2009), Scotland (Hall et al., 2019), Germany (Thiel et al., 2023), Tasmania (McIntosh et al., 2012). Paleosols and vetusols in the Yukon territory underwent a large number of glacial-interglacial cycles (Sanborn, 2016) throughout the Quaternary.

Indeed, these deep soil layers provide important paleoenvironmental information (Table 4). The presence of clay coatings (later broken by frost activity) in the Bsm(v) horizon, for example, indicates a rather long period of stable temperate and humid broadleaf environment preceding the LGM (MIS 5, or preceding periods with at least similar temperate climates). Based on the thickness and development degree, and abundance of spodic materials in Bs and Bhs horizons, the most important soil forming process, however, seems to have been podzolization, for long periods of time, in all three layers. The podzolization was particularly intense, producing large amounts of Al-SOM compounds, able to persist for many thousands of years and still detectable in the laboratory through the spodicity index. The abundance of gibbsite in the deepest horizons points to a particularly long pedogenesis as well.

5. Conclusions

The 11x3 m soil section we characterized is one of the most complete soil profile ever observed inside and between large Pleistocene blockstreams. It allowed us to detect the inner structures, which can be explained by the presence of ice-rich permafrost during the cold Pleistocene periods, and the soil horizons, which are evidences of intense podzolization during many warm interglacials as well as during the Holocene. Some soil horizons are also indicative of different climatic conditions, such as humid conditions (clay coatings observed in thin section in a cemented layer).

Old age and strong polygenesis thus have been necessary for the development of this blockstream-vegetated area-blockstream section, and for the soil formed inside it. Unfortunately, no absolute dating technique can be reasonably used for such a complex soil profile, able to quantitively confirm the pedogenic trends.

Author contributions.

Michele E. D'Amico: conceptualization, formal analysis, investigation, data curation, writing, editing. Emanuele Pintaldi: formal analysis, investigation, data curation, editing. Andrea Benech: formal analysis, investigation, editing. Chiara Colombero: formal analysis, investigation, editing. Eleonora Bonifacio, Michele Freppaz: supervision, resources, editing.

CRediT authorship contribution statement

Michele Eugenio D'Amico: Writing – review & editing, Writing – original draft, Investigation, Formal analysis, Data curation, Conceptualization. **Emanuele Pintaldi:** Writing – review & editing, Investigation, Formal analysis, Data curation. **Chiara Colombero:** Writing – review & editing, Investigation, Formal analysis. **Eleonora Bonifacio:** Supervision, Resources. **Andrea Benech:** Writing – review & editing, Investigation, Formal analysis. **Michele Freppaz:** Supervision, Resources.

Declaration of competing interest

The authors declare that they have no known competing financial interests or personal relationships that could have appeared to influence the work reported in this paper.

Acknowledgements

We thank Dr. Alexey Lupachev and its lab for the preparation and the photography of the thin section sample, and for the useful discussion in front of the soil profile. Andrea Benech acknowledges the support of NBFC to University of Turin/DISAFA, funded by the Italian Ministry of University and Research, PNRR, Mission 4 Component 2, "Dalla ricerca all'impresa", Investment 1.4, Project CN00000033.

Appendix A. Supplementary material

Supplementary data to this article can be found online at https://doi.org/10.1016/j.catena.2024.108676.

References

Andersen, J.L., Egholm, D.L., Knudsen, M.F., Linge, H., Jansen, J.D., Goodfellow, B.W., Pedersen, V.K., Tikhomirov, D., Olsen, J., Fredin, O., 2018. Pleistocene evolution of a Scandinavian plateau landscape. J. Geophys. Res.: Earth Surf. 123, 3370–3387. https://doi.org/10.1029/2018JF004670.

André, M., Hall, K., Bertran, P., Arocena, J., 2008. Stone runs in the Falklands: periglacial or tropical? Geomorph. 95, 524–543. https://doi.org/10.1016/j.geomorph.2007.07.006.

Ballantyne, C.K., 1998. Age and significance of mountain-top detritus. Perm. Perig. Process. 9, 327–345. https://doi.org/10.1002/(SICI)1099-1530(199810/12)9:4%3C327::AID-PPP298%3E3.0.CO;2-9.

Ballantyne, C.K., 2010. A general model of autochthonous blockfield evolution. Permafr. Periglac. Process. 21, 289–300. https://doi.org/10.1002/ppp.700.
Ballantyne, C.K., Harris, C., 1994. The periglaciation of Great Britain. Cambridge University Press.
Ballantyne, C.K., McCarroll, D., Stone, J.O., 2007. The Donegal ice dome, northwest Ireland: dimension and chronology. J Quat Sci. 22 (8), 773783. https://doi.org/10.1002/jqs.1116.
Barrows, T.T., Stone, J.O., Fifield, L.K., 2004. Exposure ages for Pleistocene periglacial deposits in Australia. Quat. Sci. Rev. 23 (5–6), 697–708. https://doi.org/10.1016/j.quascirev.2003.10.011.
Benedict, J.B., 1979. Fossil ice-wedge polygons in the Colorado Front Range. Geol. Soc. Am. Bull. I (90), 173–180. https://doi.org/10.1130/0016-7606(1979)90%3C173:FIPITC%3E2.0.CO;2.
Biancotti, A., Bellardone, G., Bovo, S., Cagnazzi, B., Giacomelli, L., Marchisio, C., 1998. Distribuzione regionale di piogge e temperature. Collana Studi Climatologici in Piemonte, Volume 1. Ed. Clima Icam, Torino.
Bockheim, J.G., Tarnocai, C., 1998. Recognition of cryoturbation for classifying permafrost-affected soils. Geoderma 81 (3–4), 281–293. https://doi.org/10.1016/S0016-7061(97)00115-8.
Boelhouwers, J.C., 1999. Relict periglacial slope deposits in the Hex River Mountains, South Africa: observations and palaeoenvironmental implications. Geomorph. 30, 245–258. https://doi.org/10.1016/S0169-555X(99)00033-1.
Burt, R., 2004. Soil Survey Laboratory Methods Manual. Soil Survey Investigations Report No. 42. Version 4.0. Natural Resources Conservation Service, National Soil Survey Center, Lincoln, NE.
Caine, N., 1966. The blockfields and associated features of Northeastern Tasmania. PhD thesis, Australian National University.
Carraro, F., Giardino, M., 2004. Quaternary glaciations in the western Italian Alps: a review. Development in Quaternary Science 2 (1), 201–208.
Cerbian, F.N., Poch, R., Villas, B.N., 2020. Genesis of an atypical Podzol in the Iberian Range: micromorphological characterization. SJSS. Span. J Soil Sci 10 (3). https://doi.org/10.3232/SJSS.2020.V10.N3.04.
Clark, M.G., Ciolkosz, E.J., 1988. Periglacial geomorphology of the Appalachian highlands and interior highlands south of the glacial border – a review. Geomorph. 1, 191–220. https://doi.org/10.1016/0169-555X(88)90014-1.
D'Amico, M.E., Pintaldi, E., Catoni, M., et al., 2019. Pleistocene periglacial imprinting on polygenetic soils and paleosols in the SW Italian Alps. Catena 174, 269–284. https://doi.org/10.1016/j.catena.2018.11.019.
Denny, C.S., 1956. Surficial geology and geomorphology of Potter County, Pennsylvania. Geological survey professional paper 288, Department of the Interior, US.
do Vale Lopes, D., Schaefer, C.E.G.R, Lelis Leal de Souza, J.J., Soares de Oliveira, F., Nogueira Bello Simas, F., Daher, M., Gjorup, D.F., 2019. Concretionary horizons, unusual pedogenetic processes and features of sulfate affected soils from Antarctica. Geoderma, 347, 13-24. doi: 10.1016/j.geoderma.2019.03.024.
Engel, Z., Braucher, R., Aumaitre, G., Bourlès, D., Keddadouche, K., 2020. Origin and 10Be surface exposure dating of a coarse debris accumulation in the Hruby Jesenik Mountains. Central Europe. Geomorph. 365, 107292. https://doi.org/10.1016/j.geomorph.2020.107292.
FAO (Ed.), 2006. Guidelines for Soil Description, fourth ed. FAO, Rome.
Federici, P.R., Granger, D.E., Pappalardo, M., Ribolini, A., Spagnolo, M., Cyr, A.J., 2008. Exposure age dating and equilibrium line altitude reconstruction of an Egesen moraine in the Maritime Alps, Italy. Boreas 37, 247–253. https://doi.org/10.1111/j.1502-3885.2007.00018.x.
Federici, P.R., Granger, D.E., Ribolini, A., Spagnolo, M., Pappalardo, M., Cyr, A.J., 2012. Last glacial maximum and Gschnitz stadial in the Maritime Alps according to 10Be cosmogenic dating. Boreas 41, 277–291. https://doi.org/10.1111/j.1502-3885.2011.00233.x.
Fitzpatrick, E.A., 1956. An indurated soil horizon formed by permafrost. J. Soil Sci. 7 (2), 248–257.
French, H.M., Demitroff, M., Forman, S.L., 2005. Evidence for Late-Pleistocene thermokarst in the New Jersey Pine Barrens (Latitude 39° N), Eastern USA. Permafr. Periglac. Process. 16, 173–186. https://doi.org/10.1002/ppp.520.
French, H., Shur, Y., 2010. The principles of cryostratigraphy. Earth Sci. Rev. 101, 190–206. https://doi.org/10.1016/j.earscirev.2010.04.002.
Frenot, Y., Van Vliet-Lanoë, B., Gloaguen, J.C., 1995. Particle Translocation and Initial Soil Development on a Glacier Foreland, Kerguelen Islands. Subantarctic. Arct. Alp. Res. 27 (2), 107–115. https://doi.org/10.2307/1551892.
Goodfellow, B.W., 2007. Relict non-glacial surfaces in formerly glaciated landscapes. Earth-Sci Rev. 80, 47–73. https://doi.org/10.1016/j.earscirev.2006.08.002.
Goodfellow, B.W., Stroeven, A.P., Fabel, D., Fredin, O., Derron, M.H., Bintanja, R., Caffee, M.W., 2014. Arctic-alpine blockfields in northern Swedish Scandes: late Quaternary, not Neogene. Earth Surf. Dynam. 2, 383e401. https://doi.org/10.5194/esurf-2-383-2014.
Gowan, R.J., Dallimore, S.R., 1990. Ground ice associated with granular deposits in the Tuktoyaktuk coastand area, N.W.T. Nordicana 54, 283–290.
Grab, S., 1999. Block and Debris Deposits in the High Drakensberg, Lesotho, Southern Africa: Implications for High Altitude Slope Processes. Geografiska Annaler: Series A. Phys. Geogr. 81 (1), 1–16. https://doi.org/10.1111/j.0435-3676.1999.00045.x.
Haeberli, W., Mühl, D.V., 1996. On the characteristics and possible origins of ice in rock glacier permafrost. Z. Geomorph. N. F. Suppl. BD 104, 43–57.
Hall, A.M., Merritt, J.W., Connell, E.R., Hubbard, A., 2019. Early and Middle Pleistocene environments, landforms and sediments in Scotland. Earth Environ. Transact. Royal Soc. Edinburgh 110, 5–37. https://doi.org/10.1017/S1755691018000713.
Hamilton, B.T.B., 1977. The occurrence of vesicular structures in arctic and subarctic soils. Zeitschr. Geomorph. 21 (1), 87–95.
Hansom, J.D., Evans, D.J.A., Sanderson, D.C.W., Bingham, R.G., Bentley, M.J., 2008. Constraining the age and formation of stone runs in the Falkland Islands using Optically Stimulated Luminescence. Geomorph. 94 (1–2), 117–130. https://doi.org/10.1016/j.geomorph.2007.05.006.
Harris, S.A., 1994. Climatic zonality of periglacial landforms in mountain areas. Arctic 47, 184–192. https://doi.org/10.14430/arctic1288.
Harris, S.A., Jin, H., He, R., 2017. Short Communication. Very large cryoturbation strictures of Last Permafrost Maximum age at the foot of the Qilian Mountains (NE Tibet Plateau, China): a discussion. Permafr. Perigl. Proc. 28, 757–762. https://doi.org/10.1002/ppp.1942.
Hopkinson, C., Ballantyne, C.K., 2014. Age and origin of blockfields on Scottish mountains. Scot. Geogr. J. 130 (2), 116–141. https://doi.org/10.1080/14702541.2013.855808.
Ipla, 2007. Carta dei Suoli del Piemonte 1:250000. SELCA, Firenze.
Islam, A.K.M.E., Lotse, E.G., 1986. Quantitative mineralogical analysis of some Bangladesh soils with X-ray, ion exchange and selective dissolution techniques. Clay Miner. 21, 31–42.
IUSS Working Group WRB, 2022. World Reference Base for Soil Resources. International soil classification system for naming soils and creating legends for soil maps, 4th edition. International Union of Soil Sciences (IUSS), Vienna, Austria.
Jacobsen, B.H., Siegert, C., Ostrumov, V., 1996. Effect of permafrost and paleo-environmental history on soil formation in the lower Kolyma Lowland, Siberia. Geografisk Tidsskrift 96, 40–50.
Jones, D.B., Harrison, S., Anderson, K., Whalley, W.B., 2019. Rock glaciers and mountain hydrology: a review. Earth-Sci- Rev. 193, 66–90. https://doi.org/10.1016/j.earscirev.2019.04.001.
Karte, J., 1983. Periglacial phenomena and their significance as climatic and edaphic indicators. GeoJ. 7 (4), 329–340.
Kasprzak, M., 2015. High-resolution electrical resistivity tomography applied to patterned ground, Wedel Jarlsberg Land, south-west Spitsbergen. Polar Res. 34, 25678. https://doi.org/10.3402/polar.v34.25678.
Levy, J.S., Fountain, A.G., Gooseff, M.N., Welch, K.A., Lyons, W.B., 2013. Garwood Valley, Antarctica: classification, distribution, and climate implications from HiRISE observations. J Geophys. Res. 114 (E1), E01007.
Lundström, U., van Breemen, N., Bain, D., 2000. The podzolization process. A review. Geoderma 94 (2–4), 91–107. https://doi.org/10.1016/S0016-7061(99)00036-1.
Lupachev, A., Gubin, S., 2023. The soil-cryogenic complex: evidence of late Pleistocene-Holocene coevolution of permafrost and cryosols at the Kolyma Lowland. Permafrost Periglac. Process. 34 (3), 317–330. https://doi.org/10.1002/ppp.2191.
Marr, P., Löffler, J., 2017. Establishing a multi-proxy approach to alpine blockfield evolution in south-central Norway. AUC Geographica. https://doi.org/10.14712/23361980.2017.18.
Masseroli, A., Bollati, I.M., Proverbio, S.S., Pelfini, M., Trombino, L., 2020. Soils as a useful tool for reconstructing geomorphic dynamics in high mountain environments: the case of the Buscagna stream hydrographic basin (Lepontine Alps). Geomorph. 371, 17442. https://doi.org/10.1016/j.geomorph.2020.107442.
McIntosh, P.D., Eberhard, R., Slee, A., Moss, P., Price, D.M., Donaldson, P., Doyle, R., Martins, J., 2012. Late Quaternary extraglacial cold-climate deposits in low and mid-altitude Tasmania and their climatic implications. Geomorphology 179, 21–39. https://doi.org/10.1016/j.geomorph.2012.08.009.
Merrits, D.J., Rahnis, M.A., 2022. Pleistocene Periglacial Processes and Landforms, Mid-Atlantic Region, Eastern United States. Ann. Rev. Earth Planet. Sci. 50, 541–592. https://doi.org/10.1146/annurev-earth-032320-102849.
Mirabella A., Bonifacio E., Colombo C.M. (2005). Diffrattometria a raggi X – analisi mineralogica qualitativa. In Adamo P (Ed.) Metodi di analisi mineralogica del suolo. Ministero delle Politiche Agricole e Forestali, Roma, Italy, chapter VII.3.
Müller, S., Thiemeyer, H., 2014. Formation and transformation of Pleistocene periglacial slope deposits in the Spessart Mountains (Hesse, Germany). Zeitschrift für Geomorphologie, 58. Suppl. 3, 91–113. https://doi.org/10.1127/0372-8854/2014/S-00157.
Murton, J.B., Worsley, P., Godzik, J., 2000. Sand veins and wedges in cold aeolian environments. Quat. Sci. Rev. 19, 899–922. https://doi.org/10.1016/S0277-3791(99)00045-1.
Murton, J.B., 2007. Ice wedges and ice wedge casts. SA Elias (red.), Encyclopaedia of Quaternary Sciences. https://doi.org/10.1016/B0-44-452747-8/00108-3.
Paro, L., 2011. Il ruolo dei processi criotici nell'evoluzione del paesaggio alpino: il caso di studio dei block stream del Complesso Ultrabasico di Lanzo (Alpi occidentali italiane). Relationship between cryotic processes and block streams evolution in the Lanzo Ultrabasic Complex (Western Italian Alps). Ed. Arpa Piemonte, Torino.
Pintaldi, E., D'Amico, M.E., Colombo, N., Martinetto, E., Said-Pullicino, D., Giardino, M., Freppaz, M., 2021a. Hidden paleosols on a high-elevation Alpine plateau (NW Italy): evidence for Lateglacial Nunatak? Glob. Planet. Chang. 207, 103676. https://doi.org/10.1016/j.gloplacha.2021.103676.
Pintaldi, E., D'Amico, M.E., Colombo, N., Colombero, C., Sambuelli, L., De Regibus, C., Franco, D., Perotti, L., Paro, L., Freppaz, M., 2021b. Hidden soils and their carbon stocks at high-elevation in the European Alps (North-West Italy). Catena 198, 105044. https://doi.org/10.1016/j.catena.2020.105044.
Pissart, A., 1970. Les phénomènes essentiels liés au gel, les structires périglaciares qui ne resultants et leur significationd climatique. Annales De La Societè Geologique De Belgique 93, 7–49.
Pitkäranta, R., 2009. Pre-late Weichselian podzol soil, permafrost features and lithostratigraphy at Penttilängas, western Finland. Bull. Geol. Soc. Finland 81, 53–74.
Rellini, I., Trombino, L., Rossi, P.M., Firpo, M., 2014. Frost activity and ice segregation in a palaeosol of the Ligurian Alps (Beigua Massif, Italy): evidence of past permafrost? Geogr. Fis. Din. Quat. 37, 29–42.

Rixhon, G., Demoulin, A., 2013. Evolution of slopes in a cold climate. In: Shroder, J.F. (Ed.), Treatise on Geomorphology, Vol. 8. Academic Press, San Diego, pp. 392–415.
Romanovskii, N.N., 1985. Distribution of recently active ice and soil wedges in the USSR. In: Church, M., Slaymaker, O. (Eds.), Field and Theory; Lectures in Geocryology. University of British Columbia Press, Vancouver, pp. 154–165.
Sanborn, P., 2016. The imprint of time on Canadian soil landscapes. Quat. Int. 418, 165–179. https://doi.org/10.1016/j.quaint.2015.09.053.
Schaetzl, R.K., Anderson, N.L., 2015. Soils: Genesis and Geomorphology, second edition. Cambridge University Press, Cambridge.
Scotti, R., Brandinoni, F., Alberti, S., Frattini, P., Crosta, G.B., 2013. A regional inventory of rock glaciers and protalus ramparts in the central Italian Alps. Geomorph. 186, 136–149. https://doi.org/10.1016/j.geomorph.2012.12.028.
Sedov, S., Rusakov, A., Sheinkman, V., Korkka, M., 2016. MIS3 paleosols in the center-north of Eastern Europe and Western Siberia: Reductomorphic pedogenesis conditioned by permafrost? Catena 146, 38–47. https://doi.org/10.1016/j.catena.2016.03.022.
Sharp, R.P., 1942. Periglacial involutions in Illinois. J. Geol. 50, 113–133.
Skvortsova, E.B., Shein, E.V., Romanenko, K.A., et al., 2020. Formation of Vesicular Pores in Aggregates from the Eluvial Horizon of Albic Glossic Retisol during Freeze-Thaw Cycles. Eurasian Soil Sci. 53, 913–921. https://doi.org/10.1134/S1064229320070145.
Slee, A., Barrows, T.T., Shulmeister, J., Gontz, A., Kiernan, K., Haworth, R., Clack, D., Fifield, K., 2023. The age and paleoclimate implications of relict periglacial block deposits on the New England Tablelands. Australia. Quat. Res. 111, 121–137. https://doi.org/10.1017/qua.2022.32.
Stoops, G., Marcelino, V., Mees, F., 2010. Guidelines for analysis and description of soil and regolith thin sections, Second Edition. Wiley.
Thiel, C., Kenzler, M., Stephan, H.-J., Frechen, M., Urban, B., Sierralta, M., 2023. Chronological and sedimentological investigations of the Late Pleistocene succession in Osterbylund (Schleswig-Holstein, Germany), E&G Quat. Sci. J. 72, 57–72. https://doi.org/10.5194/egqsj-72-57-2023.
Van Reeuwijk, L.P., 2002. Procedures for Soil Analysis. Technical Paper n. 9. ISBN: 90-6672-044-1.
Van Steijn, H., Boelhouwers, J., Hétu, B., 2002. Recent research on the nature, origin and climatic relations of blocky and stratified slope deposits. Progr. Phys. Geogr.: Earth Envir. 26 (4), pp352ra. https://doi.org/10.1191/0309133302.
Van Vliet-Lanoë, B., 1991a. Differential frost heave, load casting and convection: Converging mechanisms; a discussion of the origin of cryoturbations. Permafr. Periglac. Proc. 2, 123–139. https://doi.org/10.1002/ppp.3430020207.
Van Vliet-Lanoë, B., 1991b. Chronostratigraphy and paleoclimatic meaning of cryogenic deformation in the Central European loess. GeoJ. 24 (2), 157–163.
Van Vliet-Lanoë, B., 1998. Frost and soils: implications for paleosols, paleoclimates and stratigraphy. Catena 34, 157–183. https://doi.org/10.1016/S0341-8162(98)00087-3.
Vandenberghe, J., Wang, X., Vandenberghe, D., 2016. Short communication - Very large cryoturbation structures of Last Permafrost Maximum age at the foot of the Qilian Mountains (NE Tibet Plateau, China). Perm. Periglac. Proc. 27, 138–143. https://doi.org/10.1002/ppp.1847.
Vanossi, M., 1990. Alpi Liguri: 11 Itinerari. Guide Geologiche Regionali, BE-MA, Pavia.
Verrecchia, E.P., Trombino, L., 2021. A Visual Atlas for Soil Micromorphologists. Springer Nature.
Vogt, T., 1992. Western Anti-Atlas (Morocco) and Central Patagonia (Argentina) calcretes: the calcium carbonate origin. Z. Geomorphol. 84, 115–127.
Vogt, T., Larquè, P., 2002. Clays and secondary minerals as permafrost indicators: examples from the circum-Baikal region. Quat. Int. 95–96, 175–187. https://doi.org/10.1016/S1040-6182(02)00038-1.
Watson, E., Morgan, A.V., 1977. A Discussion on the Changing Environmental Conditions in GreatBritain and Ireland During the Devensian (Last) Cold Stage. Phil. Transact. Royal Soc. London. Series B. Biol. Sci. 280, 183–198.
Wilson, P., 2007. Periglacial Landforms, Rock Forms – Block/rock Streams. Encyclopedia of Quaternary Science. Elsevier.
Wilson, P., 2013. Periglacial Landforms, Rock Forms – Block/rock Streams. Encyclopedia of Quaternary Science. Elsevier.
Wilson, P., Bentley, M.J., Schnabel, C., Clark, R., Xu, S., 2008. Stone run (block stream) formation in the Falkland Islands over several cold stages, deduced from cosmogenic isotope (10Be and 26Al) surface exposure dating. J. Quat. Sci. 23, 461–473. https://doi.org/10.1002/jqs.1156.
Wilson, P., Matthews, J., Mourne, R.W., 2017. Relict blockstreams at Eseheia, Valldalen-Tafjorden, southern Norway: their nature and Schmidt hammer exposure age. Permafr. Periglac. Process. 28, 286–297. https://doi.org/10.1002/ppp.1915.